Tumor-Targeted Multimodal Optical Imaging with Versatile Cadmium-Free Quantum Dots

*Xiangyou Liu, Gary B. Braun, Haizheng Zhong, David J. Hall, Wenlong Han, Mingde Qin, Chuanzhen Zhao, Meina Wang, Zhi-Gang She, Chuanbao Cao, Michael J. Sailor, William B. Stallcup, Erkki Ruoslahti, and Kazuki N. Sugahara**

The rapid development of fluorescence imaging technologies requires concurrent improvements in the performance of fluorescent probes. Quantum dots have been extensively used as an imaging probe in various research areas because of their inherent advantages based on unique optical and electronic properties. However, their clinical translation has been limited by the potential toxicity especially from cadmium. Here, a versatile bioimaging probe is developed by using highly luminescent cadmium-free $CuInSe_2$/ZnS core/shell quantum dots conjugated with CGKRK (Cys–Gly–Lys–Arg–Lys) tumor-targeting peptides. This probe exhibits excellent photostability, reasonably long circulation time, minimal toxicity, and strong tumor-specific homing property. The most important feature of this probe is that it shows distinctive versatility in tumor-targeted multimodal imaging including near-infrared, time-gated, and two-photon imaging in different tumor models. In a glioblastoma mouse model, the targeted probe clearly denotes tumor boundaries and positively labels a population of diffusely infiltrating tumor cells, suggesting its utility in precise tumor detection during surgery. This work lays a foundation for potential clinical translation of the probe.

1. Introduction

Fluorescence imaging has become an indispensable technique in cancer research because of the informative molecular, cellular, anatomical, and functional insights it provides.[1] Although the rapid advances in fluorescence imaging owe much to new imaging technologies, further improvements in sensitivity and biological selectivity require higher performance fluorescent probes. Quantum dots (QDs) are one of the most intensively studied bioimaging probes, as they possess many inherent advantages based on their unique optical and electronic properties.[2] QDs have high quantum yields (QYs), exceptional resistance to photobleaching, and high surface area-to-volume ratio that allow efficient functionalization with biomolecular ligands.[3] They can be used in near-infrared (NIR) imaging and even multiplexed imaging owing to their tunable photoluminescence (PL), large Strokes shifts, and narrow emission.[4] For some QDs, large two-photon (TP) excitation cross-sections allow them to be used in multiphoton imaging.[5] Furthermore, QDs can be used in time-gated (TG) imaging because of the relatively long luminescence lifetime (>10 ns).[6,7] These features make it possible to achieve multimodal imaging with a single QD probe, which could combine the advantages of different imaging techniques and ultimately improve both detection sensitivity and accuracy.

Dr. X. Liu, Dr. G. B. Braun, Dr. W. Han, Dr. Z.-G. She, Prof. W. B. Stallcup, Prof. E. Ruoslahti, Prof. K. N. Sugahara
Cancer Research Center
Sanford Burnham Prebys
Medical Discovery Institute
La Jolla, CA 92037, USA
E-mail: sugahara@sbpdiscovery.org

Dr. X. Liu, Prof. K. N. Sugahara
Department of Surgery
Herbert Irving Comprehensive Cancer Center
Columbia University College of
Physicians and Surgeons
New York, NY 10032, USA

Dr. G. B. Braun, Prof. E. Ruoslahti
Center for Nanomedicine and Department of
Molecular, Cellular and Developmental Biology
University of California
Santa Barbara, CA 93106, USA

DOI: 10.1002/adfm.201503453

Prof. H. Zhong, C. Zhao
Beijing Key Laboratory of Nanophotonics and
Ultrafine Optoelectronic Systems
School of Materials Science and Engineering
Beijing Institute of Technology
Beijing 100081, P. R. China

Prof. D. J. Hall
Moores Cancer Center
Department of Radiology
University of California
San Diego, La Jolla, CA 92093, USA

M. Qin, Prof. M. J. Sailor
Department of Chemistry and Biochemistry
University of California
San Diego, La Jolla, CA 92093, USA

Dr. M. Wang, Prof. C. Cao
Research Center of Materials Science
Beijing Institute of Technology
Beijing 100081, P. R. China

A major concern for QD-based probes is their potential toxicity.[8] Most QDs used currently are binary II–VI and IV–VI QDs (e.g., CdTe, CdSe, and PbS) and their core/shell nanocomplexes, which contain highly toxic elements, especially cadmium. Any possible release or leaching of the toxic elements may cause considerable safety and environmental concerns, hindering their wider applications.[9] As such, cadmium-free I–III–VI ternary semiconductor nanocrystals, such as $CuInS_2$ (CIS) and $CuInSe_2$ (CISe), have been considered as potential alternatives to replace conventional binary QDs. Generally, the QYs of naked CIS and CISe QDs are relatively low (typically <15%) but can be dramatically increased to 60% or more by precise composition control and shell coating.[7,10,11] Passivation with an inert ZnS shell also contributes to the chemical and optical stability of the QDs and protects the QD core against oxidative degradation.[12] Although some studies on the imaging potential of the ternary QDs have been reported,[11,13] exploration of CISe/ZnS or CIS/ZnS core/shell QDs for optical imaging remains at an early stage. Furthermore, data on their in vivo stability and toxicity, circulation time, and pharmacokinetics are rarely reported due to paucity of systematic studies. The application of the cadmium-free QD probes to targeted imaging with multiple imaging modalities also remains to be explored.

Peptides are desirable targeting ligands for tumor imaging because of their small size, ease of synthesis, and low immunogenicity.[14] A large number of peptides can be conjugated onto each nanoparticle to achieve multivalency for enhanced avidity of target binding.[15] CGKRK (Cys–Gly–Lys–Arg–Lys) is a tumor-specific vascular homing peptide identified by phage display in our previous work.[16,17] We recently found that the receptor for CGKRK peptide is p32, also known as gC1qR, which is a mitochondrial protein aberrantly expressed on the surface of tumor endothelial cells and other cells in tumors, where it provides a tumor-specific target.[18] Here, we synthesized CGKRK-conjugated CISe/ZnS and CIS/ZnS QDs probes for tumor-targeted imaging and employed multiple modalities to track the accumulation of the probes in tumors. We also examined the stability, in vivo distribution, toxicity, and pharmacokinetics of the probes.

2. Results and Discussion

We developed a coating strategy for CISe/ZnS and CIS/ZnS QDs inspired by long-circulating micelles,[19] and differing from previous reports using dithiolate QD anchors or expansive polymeric intercalation structures (see details in the Supporting Information).[8] We first coated the QDs with $HS{-}(CH_2)_{11}{-}(OCH_2CH_2)_6{-}NH_2$, an amphiphilic thiol ligand which has not been described for the purpose of QD bioconjugation previously.[20] The resulting QD$-NH_2$ (Figure S1, Supporting Information) presents a hydrophilic amine tail convenient for conjugation with polyethylene glycol (PEGylation) (**Figure 1**a). PL of CISe/ZnS and CIS/ZnS QDs was retained upon phase transfer to aqueous buffer solution (Figure 1b and Figure S2a, Supporting Information). We prepared CISe/ZnS QDs emitting at 709 nm to achieve deep tissue penetration of the light for NIR imaging.[21,22] PEGylation of the QDs increased the hydrodynamic diameter, reduced the surface charge and enabled conjugation of cysteine-containing peptides such as CGKRK (Figure 1c–f).[17] The size of the PEGylated CISe/ZnS QDs (QD-PEG) was 32 nm, which increased to 36 nm after CGKRK conjugation (Figure 1d).

The CGKRK-conjugated QD-PEG (QD-PEG-P) rapidly bound to cultured MCF10CA1a human breast cancer cells, leading to strong fluorescence intensity, which depended on both the incubation time (with peak intensity at 8 h) and QD concentration (**Figure 2**a,b). The saturation plateau suggests a receptor-mediated binding process consistent with the surface display of p32 by MCF10CA1a cells.[18] QD-PEG exhibited a low level of cell binding regardless of incubation time or QD concentration, which was attributed to nonspecific binding or fluid-phase uptake. Cellular uptake specificity was further confirmed by flow cytometry (Figure 2c and Figure S2c, Supporting Information). One-photon confocal microscopy showed that QD-PEG-P entered MCF10CA1a cells and accumulated predominantly in the mitochondria consistent with known CGKRK nanoparticle behavior (Figure 2d and Figure S3, Supporting Information).[17] Neither QD-PEG-P nor QD-PEG caused notable cell toxicity (Figure S4, Supporting Information).

Stability of QD-PEG in the blood was estimated by incubating the particles in fresh plasma. No aggregation or precipitation occurred, and no significant decrease of the PL intensity was detected after 24 h incubation, which excludes the possibility of ion release from the QDs (Figure S5, Supporting Information). The stability of the colloidal and optical properties of the QDs in plasma suggested suitability for in vivo imaging. The PEGylation and anionic surface charge of the particles are likely the main contributors to the stability.[23]

The circulation half-life of QD-PEG was 6.2 h (**Figure 3**a), which is comparable to that of similarly sized gold particles coated with PEG of the same molecular weight.[24] However, it is longer than those reported for other PEGylated QDs,[25] suggesting that our strategy for surface modification, including but not limited to PEGylation, provided sufficient surface passivation to protect the QDs from rapid clearance. The half-life of QD-PEG-P was 6.6 h (Figure 3a), similar to that of QD-PEG. Appropriately extending the blood circulation time is important because it provides more time for the QDs to find their target before clearance.

We next investigated the biodistribution and clearance of the QDs in mice by ex vivo imaging. The in vivo distribution and clearance of the particles are largely dependent on the particle size, surface properties such as surface charge, and the PEG chain length.[23,26] Intravenously injected QD-PEG primarily distributed into the liver and spleen and was cleared in about 9 d (Figure 3b and Figure S6a,c, Supporting Information). The heart and brain never exhibited a detectable QD signal. The lungs and kidneys showed weak signals at 24 h and almost none at 9 d postinjection (Figure S6a, Supporting Information). QD-PEG-P showed similar biodistribution in nontumor bearing mice (Figure 3c and Figure S6b,c, Supporting Information). No significant differences in the accumulation to the liver, spleen, and kidneys of QD-PEG and QD-PEG-P groups were detected (Figure S6c, Supporting Information). Generally, particles with a hydrodynamic size of less than 5.5 nm are rapidly cleared by the kidney.[27] Since the QD-PEG and QD-PEG-P

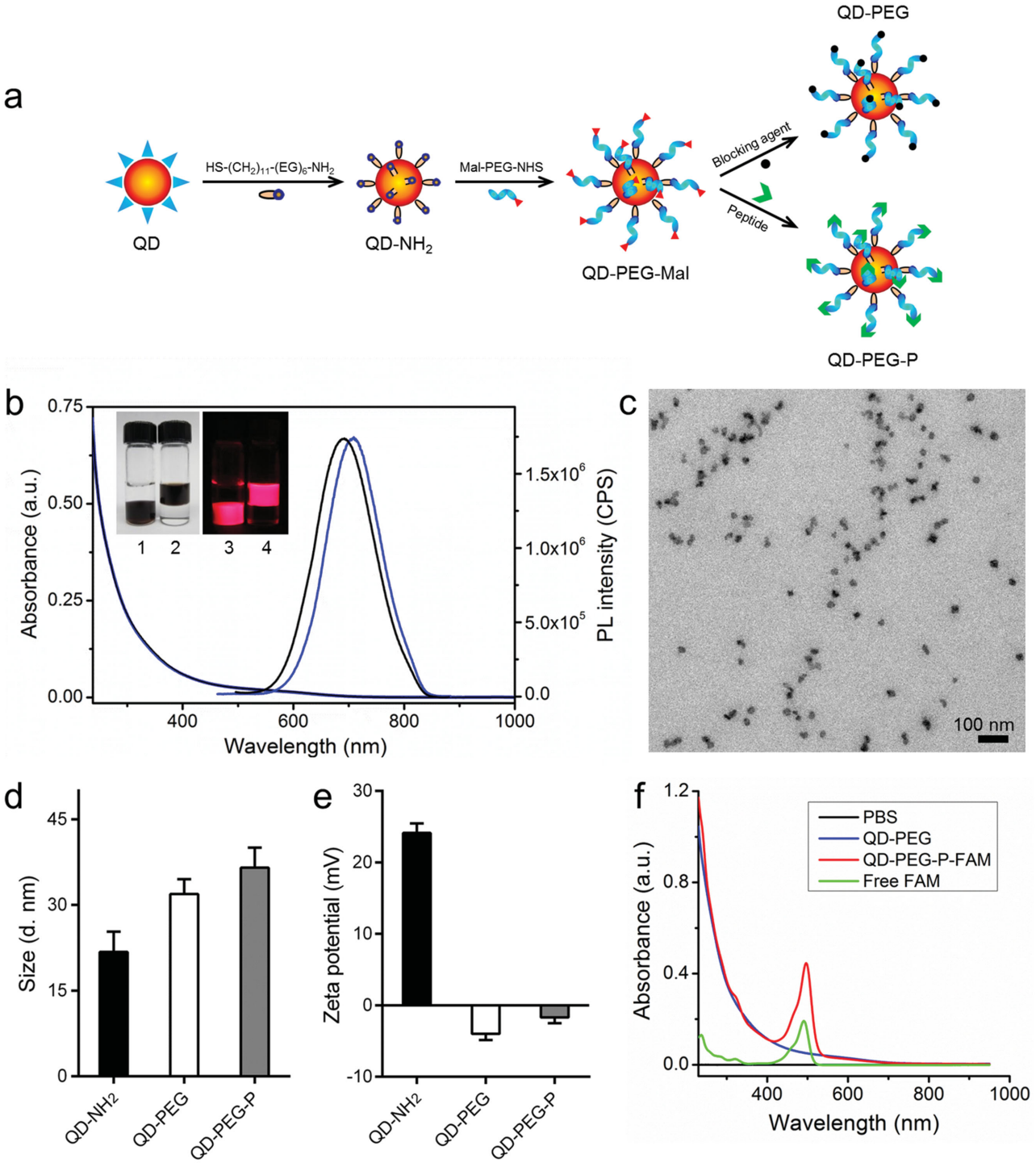

Figure 1. Preparation, characterization, and surface modification of QDs. a) Scheme for PEGylation and peptide conjugation of the QDs. b) Absorbance and PL spectra of CISe/ZnS QDs in chloroform (black) and QD—NH_2 in PBS (blue). Emission peaks are at 692 nm (black) and 709 nm (blue), respectively. The insets are images of CISe/ZnS QDs before (1,3) and after phase transfer (2,4), taken under ambient light (1,2) or under 365 nm UV light (3,4). Each vial contains two solvent layers: at the top is PBS and at the bottom is chloroform. c) TEM image of QD—NH_2 in PBS. d,e) Hydrodynamic diameter and Zeta potential of the QD samples. f) Absorbance spectra of QD-PEG (blue), QD-PEG-P-FAM (fluorescein) (red), and free FAM (green) in PBS. FAM-CGKRK was used here instead of unlabeled CGKRK in order to verify the conjugation of the peptide onto the QDs. After extensive washing to remove nonconjugated peptide, significant FAM peak at around 495 nm could be detected, validating the conjugation method.

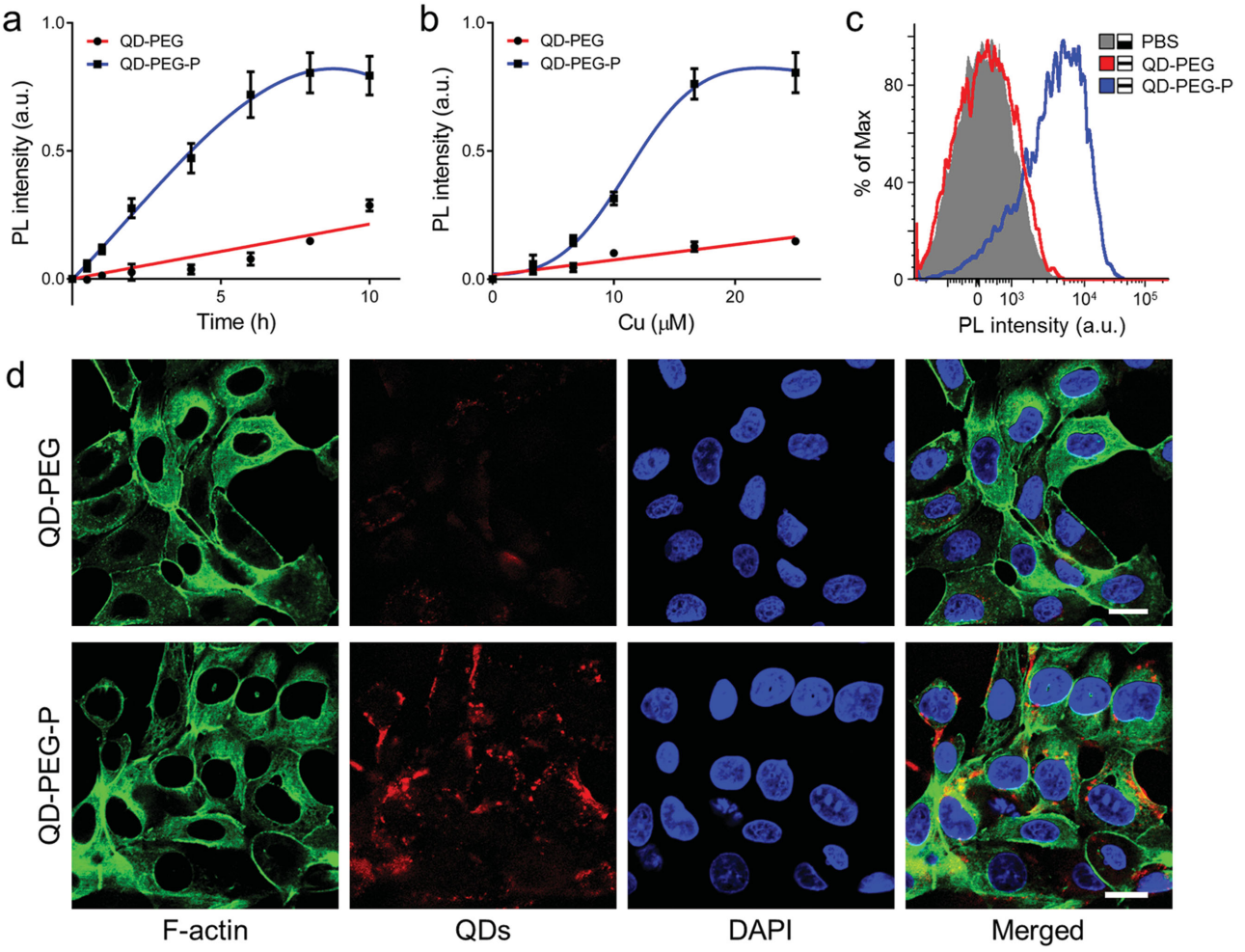

Figure 2. In vitro cell labeling with QDs. a–c) Time- and concentration-dependent QD binding to MCF10CA1a human breast cancer cells quantified with a,b) a fluorescence plate reader and c) a flow cytometer. d) One-photon confocal images of MCF10CA1a cells treated with QD-PEG (25×10^{-6} M) or QD-PEG-P (25×10^{-6} M) for 4 h. F-actin staining outlines the cells. Scale bars: 20 μm.

particles are larger than 5.5 nm, they are unlikely to be primarily cleared by renal filtration unless degraded, which may explain their low distribution in kidneys. These results suggest that hepatic clearance may be the primary pathway of elimination. The efficient clearance may help avoid possible chronic toxicities caused by residual QDs. In fact, neither significant differences in blood biochemical parameters nor pathological changes were detected in the QD-PEG and QD-PEG-P groups compared with control (phosphate buffered saline, PBS) group at 24 h or one week after a single injection (Figure 3d and Figures S7 and S8, Supporting Information). These data suggest that the QDs are well tolerated in mice, owing to their surface PEGylation, lack of toxic elements, and efficient clearance in a reasonable timescale.

To demonstrate the potential of the QDs for targeted in vivo imaging, NIR imaging with live mice bearing orthotopic MCF10CA1a xenograft tumors was performed over time (Figure S9, Supporting Information). Control mice (PBS group) showed minimal signal in the tumor with some background autofluorescence appearing at ≈6–12 h, which is ascribed to food intake. Significant QD signal was detected in the tumors of mice injected with QD-PEG-P. The signal appeared as soon as 30 min postinjection, indicating rapid accumulation of QD-PEG-P in tumors. In contrast, the QD-PEG tumors were only weakly positive at 30 min, likely because of nonspecific retention of the particles either in tumor tissue or vessels.

QD-PEG-P signal in the tumors increased over the first 3 h after injection and remained stable for the next 25 h (Figure S9a,b, Supporting Information). Particularly, from 24 h postinjection, the QD-PEG-P signal became predominant in the tumor with much lower signals in nontumor tissues. The long retention of the targeted QDs suggested strong interaction with tumor tissue and high in vivo stability, properties suitable for in vivo imaging. In contrast, the QD-PEG-P signal in nontumor tissues exhibited faster changes. The QD-PEG-P signals in nontumor tissues peaked at ≈12 h and decreased to background level at 28 h postinjection (Figure S9a, Supporting Information). Similar changes occurred in the QD-PEG group. The strong signals in nontumor tissues at earlier time points was likely due to clearance of circulating off-target QDs by the

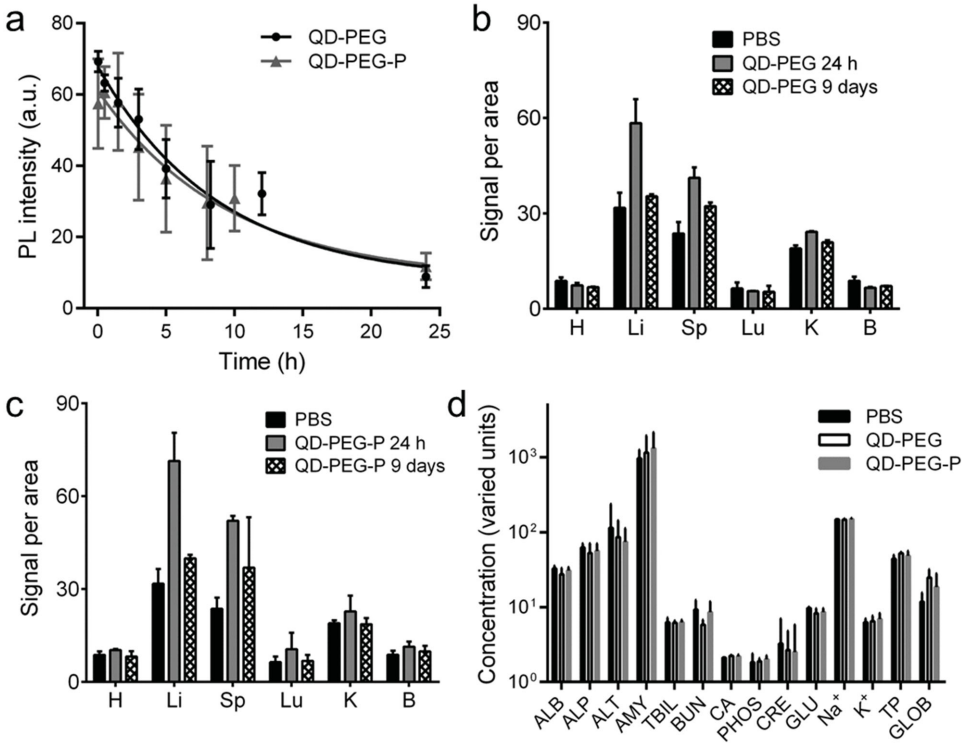

Figure 3. Circulation time, distribution, and blood chemistry of QDs in vivo. a) Plasma concentrations of QD-PEG and QD-PEG-P at different time points after intravenous injection, $n = 9$ mice per group. b,c) Quantification of the QD signal per area in each tissue based on the ex vivo imaging results (see Figure S6a,b, Supporting Information) of b) QD-PEG or c) QD-PEG-P treated mice, $n = 3$ mice per group. H, heart; Li, liver; Sp, spleen; Lu, lung; K, kidney; B, brain. d) Blood chemistry was evaluated 24 h after the injection of PBS (control), QD-PEG or QD-PEG-P, $n = 4$–6 mice per group. Differences between QD-PEG or QD-PEG-P versus PBS group were not significant with a criterion of $P < 0.05$ for significance. ALB, albumin (g L^{-1}); ALP, alkaline phosphatase (units L^{-1}); ALT, alanine transaminase (units L^{-1}); AMY, amylase (units L^{-1}); TBIL, total bilirubin (μM); BUN, blood urea nitrogen (mM); CA, calcium (mM); PHOS, phosphorus (mM); CRE, creatinine (μM); GLU, glucose (mM); Na^+, sodium (mM); K^+, potassium (mM); TP, total protein (g L^{-1}); GLOB, globulin (g L^{-1}).

reticuloendothelial system.[26,27] The highest tumor-to-background ratio arose in the QD-PEG-P group at ≈24 h (Figures S9c and S10, Supporting Information), apparently owing to the high accumulation in and slow clearance from the tumor compared to normal tissues. Although there was passive accumulation of QD-PEG in the tumor, the signal was about 70% lower than that in the QD-PEG-P group (Figure S9b, Supporting Information). The background signal in the QD-PEG and QD-PEG-P groups at 28 h (**Figure 4**a) is attributed to residual QDs in the blood. The high sensitivity and selectivity of the QD-PEG-P probe makes it suitable for tumor-targeted NIR imaging in live animals.

Ex vivo continuous wave (CW) imaging of tissues collected at the end of the in vivo imaging experiment confirmed the extensive accumulation of QD-PEG-P in tumors and low background in other tissues except liver (Figure 4b, CW panel). The liver signal was confounded by tissue autofluorescence, as the livers from the PBS-injected mice were also positive. This problem was solved using TG imaging (Figure 4b, TG panel), which selectively eliminates short-lived (<10 ns) autofluorescence while leaving long-lived luminescent signals.[6] I-III-VI QDs have a longer PL lifetime than conventional binary II-VI QDs (100–300 ns vs 10–20 ns),[7] suggesting that ternary QDs could be superior for TG imaging.[28] As expected, much cleaner background was obtained with TG imaging (Figure 4b), and the highest signal was detected in the QD-PEG-P tumor, consistent with the in vivo imaging results in Figure 4a. Inductively coupled plasma optical emission spectroscopy (ICP-OES) measurements showed approximately twofold more indium in the QD-PEG-P tumors than in the QD-PEG tumors (Figure 4c). One-photon confocal microscopy revealed significant QD signal in tumor sections from the QD-PEG-P mice, whereas little signal was detected in the QD-PEG tumor sections (Figure 4d) and the liver or kidney from the QD-PEG-P mice (Figure S11, Supporting Information). The much lower QD-PEG signal in tumor was probably due to the limited enhanced permeability and retention effect. Notably, most of the QD-PEG-P particles were observed in the tumor interstitium around the vasculature (Figure 4d). These results demonstrate strong tumor-homing activity and suitability for optical imaging of QD-PEG-P in the MCF10CA1a tumor model.

Two-photon imaging also confirmed the tumor-specific accumulation of QD-PEG-P in the MCF10CA1a tumors. TP excitation with NIR wavelength allows imaging of thick tissues with low autofluorescence.[5,22] CISe/ZnS (and CIS/ZnS) QDs are suitable for TP imaging according to the TP activities, which were verified by measuring the dependence of PL intensity

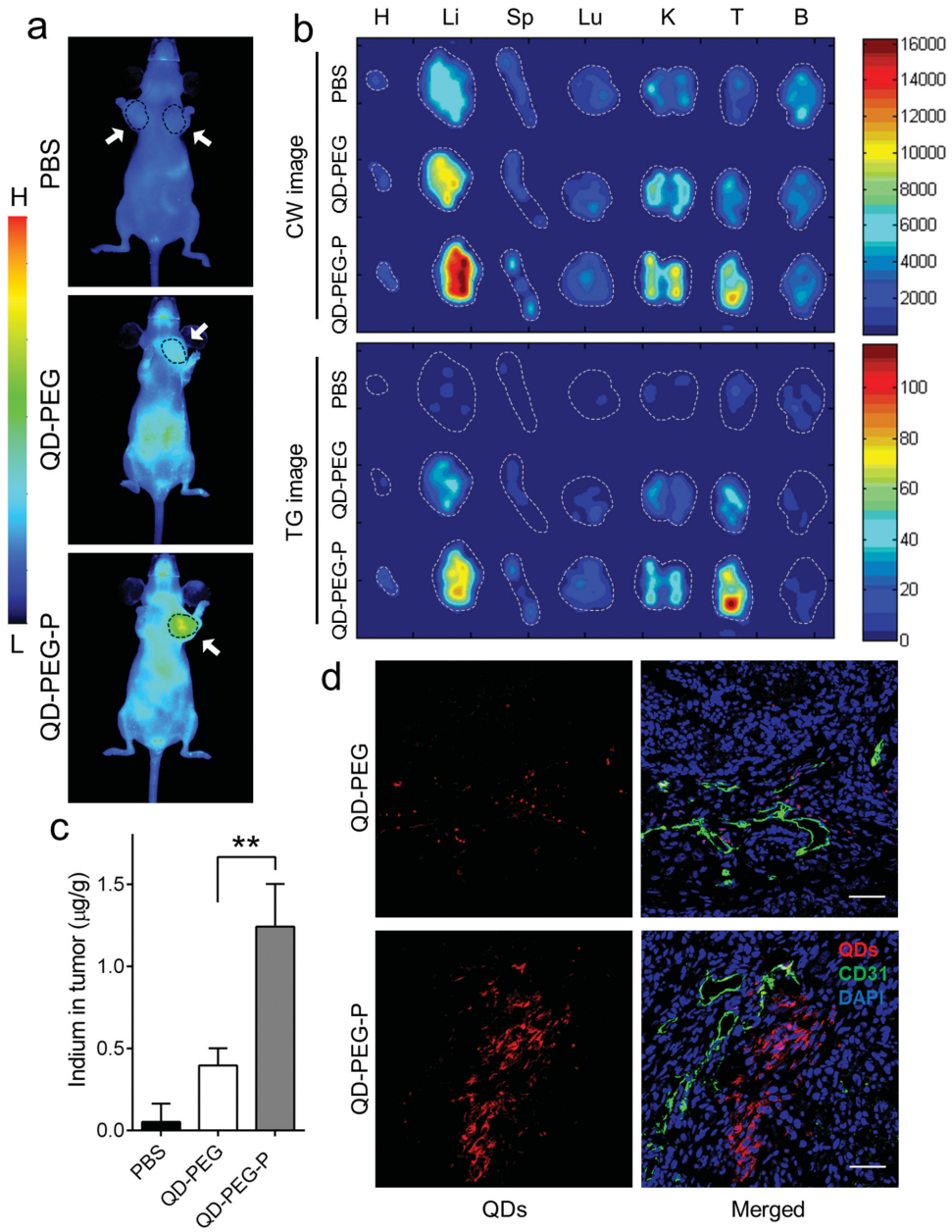

Figure 4. Breast tumor targeting with QD-PEG-P. a) Intravital whole body fluorescent imaging (ventral view) of MCF10CA1a breast-tumor-bearing nude mice at 28 h after intravenous injection of PBS, QD-PEG, or QD-PEG-P. Images were taken under 700 nm channel of Li Cor Pearl Impulse small animal imaging system. White arrows show the position of MCF10CA1a tumors (circled in black). b) Ex vivo CW and TG imaging of the tissues harvested from the mice in (a) after the in vivo imaging. H, heart; Li, liver; Sp, spleen; Lu, lung; K, kidney; T, tumor; B, brain. c) Quantitative analysis of indium in the tumors by ICP-OES, $n = 3$ in each group. $^{**}P < 0.01$. d) Representative confocal microscopy images of QD distribution in sections from the tumors in panel (b). Scale bars: 50 μm.

on the incident power and the PL spectra upon TP excitation (Figures S2b,d and S12a,b, Supporting Information). 3D TP microscopy of MCF10CA1a cells grown in 2D culture provided exceptionally clear images of QD-PEG-P within the cells (Figure S12c, Supporting Information). TP microscopy on 60 μm thick MCF10CA1a tissue sections revealed extensive 3D distribution of QD-PEG-P and minimal QD-PEG accumulation (Figure S12d,e, Supporting Information). These results demonstrate the utility of QD-PEG-P in TP imaging and confirm the capability of QD-PEG-P as a tumor-targeting probe.

Finally, the QD-PEG-P probe was tested in mice bearing brain tumors established by intracranial microinjection of NG2-positive mouse glioma cells expressing green fluorescent protein (GFP-CT2A).[29] CGKRK effectively targets the vasculature and tumor cells in glioblastoma.[17] In fact, QD-PEG-P extensively bound to GFP-CT2A cells in vitro (Figure S13,

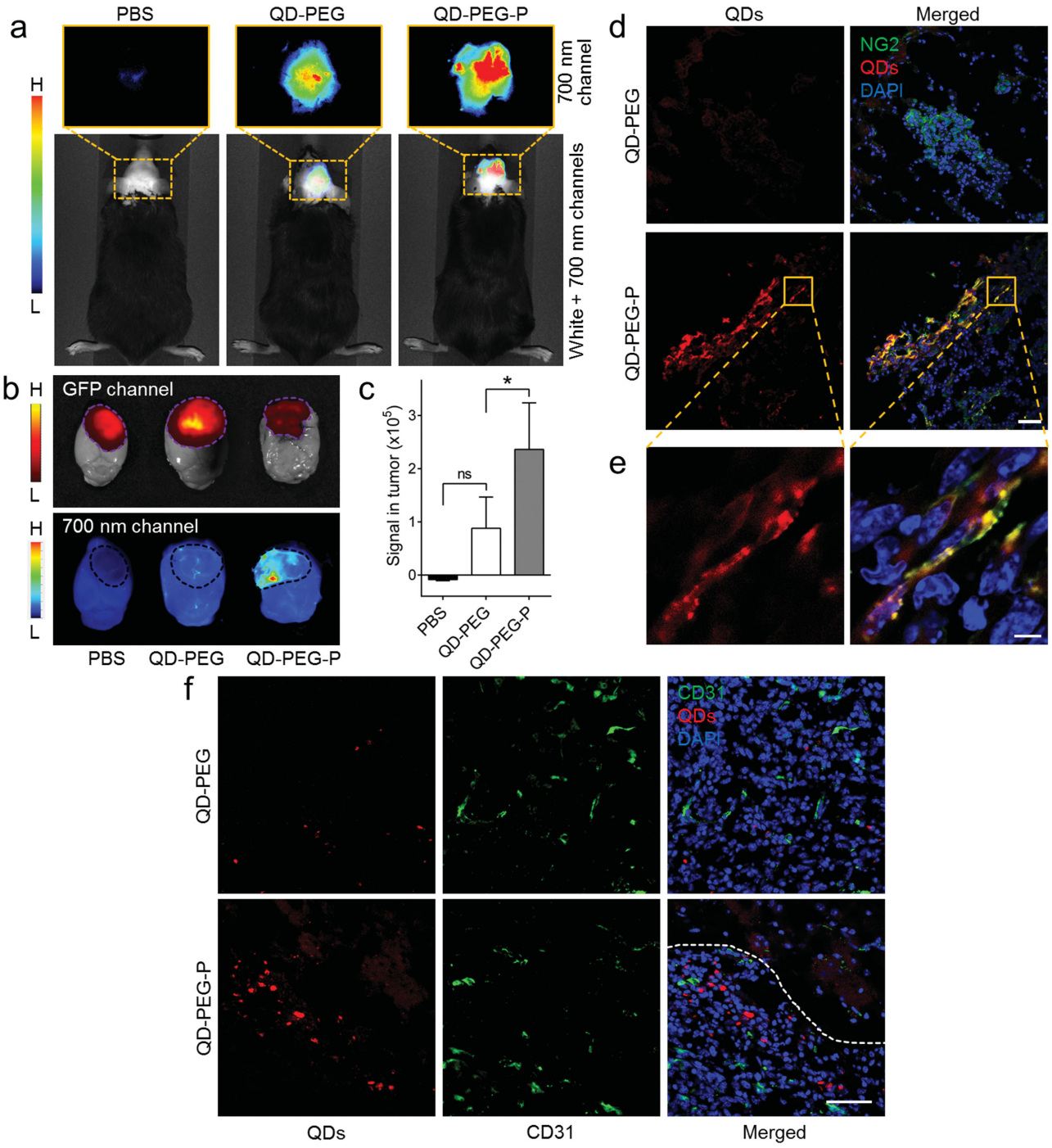

Figure 5. Brain tumor targeting with QD-PEG-P. a) Intravital whole body fluorescent imaging (dorsal view) of the brain tumor-bearing mice injected with PBS, QD-PEG, or QD-PEG-P. Tumor mice with shaved head were imaged at 3.5 h postinjection using the 700 nm channel of Li Cor Pearl Impulse small animal imaging system. b) Ex vivo fluorescent imaging of brains excised from the mice imaged in (a). The upper panel image was obtained with Xenogen IVIS200 imaging system, and the lower panel one was with a Li Cor Odyssey CLx infrared imaging system. c) Quantification of the 700 nm channel signals from tumors, $n = 3$ in each group. $^*P < 0.05$. d–f) Representative confocal microscopy images of QD distribution in sections from the brains in panel (b). The sections were immunostained with either d,e) NG2 antibody (green) or f) endothelial cell marker CD31 antibody (green). e) Magnified images corresponding to the square areas in the QD-PEG-P group in (d). White dashed line in (f) indicates the tumor boundary in brain, where normal brain is above the line. Scale bars: d) 40 μm, e) 5 μm, f) 50 μm.

Supporting Information). For glioblastoma-bearing mice, strong PL signals in the brain were detected through the intact scalp and skull of mice injected with QD-PEG-P (**Figure 5**a and Figure S14, Supporting Information); the signal in brain of the QD-PEG group was lower, and the PBS group did not show any significant signal. No QD signals were detected in the

torso in the dorsal view (Figure S14, Supporting Information). Subsequent ex vivo imaging revealed the strongest PL signals in the QD-PEG-P group (Figure 5b). The signal colocalized with the GFP-positive tumor. Neither QD-PEG nor QD-PEG-P gave any signal in normal brains, consistent with the results in Figure 4b and Figure S6 (Supporting Information). These results indicate that QD-PEG-P specifically homes to glioblastoma. The QD-PEG-P signal in the brain tumor was approximately twofold higher ($P < 0.05$) than the QD-PEG signal (Figure 5c). Immunofluorescence confirmed the colocalization of QD-PEG-P with NG2-positive tumor cells (Figure 5d,e). NG2 can also be found on pericytes, cells outside the tumor, and normal blood vessels; however, we did not find QD signals in normal brain regions (Figure 5f, above the dashed line). In Figure 5f, we found only weak colocalization of QD-PEG-P with the endothelial cell marker CD31, which further suggests that QD-PEG-P targets the tumor extravascular regions including the tumor cells themselves. Remarkably, QD-PEG-P highlighted the tumor boundaries and even the so-called "guerilla" tumor cells that diffusely infiltrate at the invasion front (Figure 5d–f), suggesting its utility in precise tumor detection during surgery.

3. Conclusions

To conclude, we have developed a versatile biocompatible probe based on luminescent Cd-free CISe/ZnS QDs conjugated with a tumor-targeting CGKRK peptide through a PEG linker. The targeted QDs showed high photostability, reasonably long circulating half-life, minimal toxicity, and strong tumor-specific homing. The targeted QDs enabled noninvasive real time imaging of the tumor homing process in live mice for a long period of time. Microscopically, they provided clear intratumoral signal with TP imaging, and even allowed single cell tracking at the invasion front of glioblastoma. The NIR, TG, and TP luminescence imaging results demonstrated the suitability of these QDs for multimodality imaging, which can increase the reliability of imaging, by excluding artifacts and improving the resolution and sensitivity. As the PL spectra of the QD probes are tunable, it should also be possible to achieve multiplexed imaging. These properties suggest wide applicability of the targeted QDs in research and potentially in the imaging of human conditions amenable to optical detection.

4. Experimental Sections

Cell Lines and Animals: MCF10CA1a human breast cancer cells[18] and NG2-positive GFP-CT2A mouse astrocytoma cells were cultured in Dulbecco's modified Eagle's medium supplemented with 10% fetal bovine serum (FBS), 100 U mL^{-1} penicillin, and 100 μg mL^{-1} streptomycin. GFP-CT2A cells were generated by infecting CT2A cells[29] with GFP-expressing lentivirus. Female BALB/c mice (Harlan Laboratories), female athymic nude mice (Harlan Laboratories), and female C57BL/6 mice (Jackson Laboratory) were maintained in the vivarium of Sanford Burnham Prebys Medical Discovery Institute. All animal procedures were carried out according to a protocol approved by the Institutional Animal Care and Use Committee of the Institute.

Synthesis of CISe/ZnS QDs: CISe/ZnS QDs were synthesized based on our recently reported procedures with some modifications.[30] Copper(I) iodide (CuI, 1 mmol) and indium(III) acetate ($In(OAc)_3$, 4 mmol) were mixed with 1-dodecanethiol (2 mL) and 1-octadecene (ODE, 6 mL). The reaction mixture was degassed under vacuum for 20 min at 100 °C. After that, oleic acid (1 mL) was added into the mixture. The solution was then heated to 180 °C before the injection of selenium stock. Selenium stock solution was first prepared as follows. Selenium powder (4 mmol) and tri-*n*-octylphosphine (1.784 mL, 4 mmol) were mixed with ODE (5 mL) and oleylamine (OLA, 100 μL). The mixture was degassed under vacuum for 20 min at 130 °C. Subsequently, selenium stock was injected into the reaction mixture. After that, the reaction mixture was heated to 200 °C and kept at this temperature for 20 min with the protection of nitrogen. Zinc stock solution was prepared before this step as follows. The mixture of zinc acetate ($Zn(OAc)_2$, 10 mmol), OLA (10 mL), and ODE (10 mL) was degassed for 20 min. Next, the solution was heated to 130 °C until a clear colorless solution was formed. Then, zinc stock solution (20 mL) was added dropwise into the reaction mixture. Afterward, the reaction solution was cooled to room temperature (RT) and precipitated by adding excess acetone. The flocculent precipitate was centrifuged at 6000 rpm for 5 min and the supernatant was decanted. This process was repeated for at least three times and the precipitate was then dispersed in a nonpolar solvent (toluene or chloroform) or dried to powder.

Synthesis of CIS/ZnS QDs: Hydrophobic CIS/ZnS QDs were synthesized as previously reported.[31]

Functionalization and Characterization of QDs: Phase transfer and surface functionalization of the QDs were achieved simultaneously by mixing the QDs (20 mg QDs powders) with $HS—(CH_2)_{11}—(OCH_2CH_2)_6—NH_2$ ligands (30 mg, Prochimia) in chloroform and shaking overnight at 50 °C under inert atmosphere. After removing chloroform via nitrogen purging, 2-(*N*-morpholino) ethanesulfonic acid buffer (0.1 M, pH6.2) was added to resuspend the QDs, followed by washing with chloroform several times. Amicon Ultra-4 10K centrifugal filters were used to further purify the QDs via ultrafiltration in PBS. After centrifuging (15 000g, 10 min, 4 °C), the supernatants containing the dispersed QDs were collected and passed through 0.22 μm Millipore syringe filters. The amine-functionalized QD product ($QD—NH_2$) in PBS (1 mL, 0.6×10^{-3} M) was subsequently reacted with 2 kDa maleimide PEG N-hydroxylsuccinimide (15 mg, JenKem) for 1 h at RT, followed by purification through a Sephadex G-25 column. The QDs with attached maleimide were immediately mixed with acetyl-CGKRK peptide (7 mg) or the blocking agent *N*-acetyl-L-cysteine methyl ester (1.9 mg, Sigma-Aldrich) in PBS. The thiol maleimide reaction was allowed to proceed at 4 °C overnight. The product was purified through a Sephadex G-25 column to remove free peptide or blocking agent.

The concentrations of all QDs samples described in this paper are expressed in terms of Cu concentration unless otherwise stated. Transmission electron microscopy (TEM) observation was performed on a JEOL JEM-1200EX II electron microscope operating at 80 kV. High resolution TEM images were taken on a JEM-2100F electron microscope with an acceleration voltage of 200 kV. Dynamic light scattering (Malvern Zetasizer Nano ZS90) was used to determine the hydrodynamic size and zeta potential of the samples. Absorbance and PL spectra were measured with Beckman Coulter DU800 spectrophotometer and HORIBA FluoroMax-4 spectrofluorometer, respectively.

In Vitro Cytotoxicity, Cellular Uptake, and Imaging: A Cell Counting Kit-8 assay kit (Dojindo, USA) was employed to evaluate the toxicity of the samples according to the manufacturer's instructions and our previous reports.[32]

To study the cellular uptake of the QDs samples over time, MCF10CA1a cells were seeded into 96-well solid black plates (7×10^4 cells $well^{-1}$) and cultured overnight. QD-PEG or QD-PEG-P (25×10^{-6} M) was then added into each well. After incubation at 37 °C for various times ranging from 0.5 to 12 h, the cells were washed with PBS three times. The PL intensity at 675 nm in each well, with an excitation wavelength (Ex) of 450 nm, was measured with FlexStation 3 multimode microplate reader (Molecular Devices). To study the cellular uptake as a function of QDs' concentration, similar procedures were employed, except that the incubation time was fixed at 8 h while the concentration of QD-PEG and QD-PEG-P was varied from 0 to 25×10^{-6} M. Flow cytometry data were

acquired on FACSCanto (BD Biosciences, San Jose) after the cells had been incubated with QD-PEG or QD-PEG-P (both 25×10^{-6} M) for 4 h at 37 °C.

Samples for in vitro MCF10CA1a cell imaging were prepared by incubating the cells with QD-PEG or QD-PEG-P (both at 25×10^{-6} M) for 4 h at 37 °C, followed sequentially by three PBS washes, fixation with 4% paraformaldehyde (PFA) for 20 min, three PBS washes, permeabilizing with 0.25% Triton X-100 for 10 min, three PBS washes and treatment with 1% BSA (bovine serum albumin) for 30 min. Subsequently, the cells were stained with Acti-stain 488 phalloidin (200×10^{-9} M, Cat. No. PHDG1, Cytoskeleton) for 30 min. After PBS washes, mounting media with DAPI (4′,6-diamidino-2-phenylindole, Cat. No. H-1500, VECTASHIELD) was added. To study the subcellular distribution of QD-PEG-P, MCF10CA1a cells were treated with QD-PEG-P (25×10^{-6} M) for 3 h at 37 °C. The cells were then rinsed with PBS and stained with MitoTracker Green FM (200×10^{-9} M, Cat. No. M7514, Life technologies) for 25 min at 37 °C. After Hoechst 33342 (5 μg mL^{-1}, Life technologies) staining for 20 min, the cells were rinsed with PBS and imaged immediately. One- and two-photon imaging were both performed on Zeiss LSM 710 NLO confocal microscope equipped with Mai-Tai Laser HB (690–1020 nm). For one- and two-photon imaging, the CISe/ZnS QDs samples were excited at 561 and 900 nm, respectively, while CIS/ZnS QDs samples were excited at 514 and 820 nm. Samples for in vitro GFP-CT2A cell imaging were prepared by incubating the cells with QD-PEG or QD-PEG-P (both at 20×10^{-6} M) for 1 h at 37 °C, followed by PBS wash and Hoechst 33342 staining. After washing, live cell imaging was immediately performed.

Ex Vivo TP Imaging: MCF10CA1a cells were used to inoculate nude female mice to grow breast tumor. When tumors were ≈0.8 cm in diameter, they were excised, and cut into several pieces under ice cold Hank's balanced salt solution (HBSS). Tumor pieces were then incubated with QD-PEG (60×10^{-6} M) or QD-PEG-P (60×10^{-6} M) for 5 h at 37 °C in 24-well plate in Ham's F-12 media containing 20% FBS, 100 U mL^{-1} penicillin, and 100 μg mL^{-1} streptomycin. After the incubation, the tumor pieces were washed with PBS, fixed with 4% PFA for 2 h, dehydrated in 30% sucrose overnight, frozen in Optimal Cutting Temperature compound (OCT), and sliced into to ≈60 μm sections. The sections were treated with 0.25% Triton X-100 for 30 min, washed thrice with PBS, mounted in mounting medium with DAPI, and observed under Zeiss LSM 710 NLO confocal microscope (For DAPI, Ex is 740 nm, and emission (Em) in 410–480 nm was collected; for QDs, Ex is 850 nm, and Em in 630–700 nm was collected).

In Vitro Stability in Plasma: To test the stability of QD-PEG in plasma, QD-PEG in PBS (350×10^{-6} M) were diluted in a volume ratio of 1:3 with fresh mouse plasma and incubated in 37 °C water bath for various times ranging from 0 to 24 h. The PL intensity at 685 nm (Ex = 450 nm) was measured by FlexStation 3 multimode microplate reader (Molecular Devices).

In Vivo Toxicity, Circulation, and Distribution: To evaluate in vivo toxicity, a blood biochemistry assay was employed.[33] PBS (100 μL, as blank control), QD-PEG or QD-PEG-P in PBS (100 μL, 2 nmol QD/g body weight) was injected through the tail vein into BALB/c female mice six to eight weeks of age. Blood was collected from the retroorbital plexus of each mouse into lithium-heparin 1.3 mL micro tubes (Sarstedt) at 24 h or one week postinjection and plasma was isolated by centrifugation. The plasma (100 μL) was pipetted into Comprehensive Diagnostic Profile Rotor (Product Part No. 500-1038, Abaxis) and analyzed using VetScan VS2 chemistry analyzer. After blood collection, the mice were perfused with PBS, and tissues of interest were harvested and processed for H&E staining.

To measure the circulation half-life of QD-PEG and QD-PEG-P, blood was collected from the mice into plasma separator tubes with lithium heparin (BD Microtainer) at different time points after intravenous injection of PBS (100 μL), QD-PEG or QD-PEG-P in PBS (100 μL, 2 nmol QD/g body weight). The PL intensities of plasma at 680 nm (Ex = 450 nm) were measured with FlexStation 3 multimode microplate reader (Molecular Devices) and plotted against circulation time. The circulation half-life was determined by fitting the data to one phase exponential decay using GraphPad Prism.

To study the tissue distribution and clearance of QD-PEG and QD-PEG-P, the mice were fully anesthetized with intraperitoneal injection of Avertin at 12 h, 24 h, or 9 d after injecting PBS (100 μL), QD-PEG or QD-PEG-P in PBS (100 μL, 2 nmol QD/g body weight). Tissues were harvested after perfusion with PBS, followed by ex vivo imaging using the 700 nm channel of the Odyssey CLx infrared imaging system (Li Cor). The results were quantified by measuring the signal per area in each tissue with Li Cor Image Studio Lite 4.0 software.

Breast Tumor Model and Imaging: Breast tumors were generated by injecting 10^6 MCF10CA1a cells into the mammary fat pad of nude female mice. When the tumors had grown to a size about 0.4 cm^3, PBS (100 μL), QD-PEG, or QD-PEG-P in PBS (100 μL, 2 nmol QD/g body weight) was injected intravenously. The mice were then imaged with the Li Cor Pearl Impulse small animal imaging system, and the results were quantified with Li Cor Image Studio Lite 4.0 software. At 28 h after injection, the mice were perfused with PBS, and tissues were collected and imaged with a preclinical in vivo time-domain fluorescence imaging system, eXplore Optix (GE&ART Advanced Research Technologies, Inc.). CW fluorescence intensity images were obtained from all detected photons whereas TG fluorescence intensity images were generated only from photons arriving ≈9 ns after the excitation pulse (thus avoiding autofluorescence at a time when only the QD signal persists).

After ex vivo TG imaging, the tissues were fixed with 4% PFA for 2 h, cryoprotected in 30% sucrose overnight, frozen in OCT, and sliced into 7 μm sections. The sections were treated with 0.25% Triton X-100 for 10 min, washed with three times with PBS, blocked with 1% BSA for 1 h, and incubated with rat antimouse CD31 primary antibody (BD Biosciences) at 4 °C overnight, followed by Alexa Fluor 488 goat antirat IgG secondary antibody (Life technologies) for 1 h. After washing with PBS, sections were mounted in DAPI-containing mounting medium and examined under Zeiss LSM 710 NLO confocal microscope. In parallel experiments, tissues were processed for ICP-OES measurement.[34] Tissues were digested at 75 °C for 3 h in *aqua regia* containing 0.4 μg mL^{-1} of yttrium as an internal standard, followed by treatment with hydrogen peroxide at RT for ≈1 h until the solution became colorless. The digested solutions were then heated at 75 °C for another 0.5 h. After centrifugation (10 000g, 10 min), the supernatants were diluted with Milli-Q water, and indium content was quantified with ICP-OES (Perkin-Elmer Optima 3000 DV) to determine the distribution of QDs in each tissue.

Intracranial Microinjection and Growth of Brain Tumors: Brain tumor model was established according to procedures described previously with minor modifications.[29] NG2-positive GFP-CT2A astrocytoma cells were harvested and resuspended in PBS at a density of 2.5×10^7 cells mL^{-1}. From this suspension, 2 μL (5×10^4 cells per mouse) were microinjected into the forceps minor of the corpus callosum (stereotactic coordinates relative to bregma: 2 mm lateral, 1 mm rostral, 2.5 mm deep) of female mice (ten to twelve weeks old) under Avertin anesthesia. An injection rate of 0.2 μL min^{-1} was maintained with the use of a Stoelting micropump connected to a 10 μL Hamilton syringe with a 26-gauge needle. Animals were monitored daily for signs of distress, such as weight loss, seizures, posturing, and nasal and/or periorbital hemorrhage. No mice in our study exhibited these symptoms.

Brain Tumor Imaging: At 24 days after injection of GFP-CT2A cells, the mice were intravenously injected with PBS (100 μL), QD-PEG or QD-PEG-P in PBS (100 μL, 2 nmol QD/g body weight). At 3.5 h after the injection, the mice, with their heads shaved, were imaged at 700 nm channel with the Li Cor Pearl Impulse small animal imaging system. After imaging, the mice were perfused under Avertin anesthesia. Brains were excised for ex vivo imaging with Xenogen IVIS200 imaging system to detect GFP signal from the CT2A cells, then with Li Cor Odyssey CLx infrared imaging system to detect the QD signals. The images were quantified based on PL intensities of the QDs in the tumors. After ex vivo imaging, the brains were fixed and treated as described above to collect sections for immunofluorescent staining. Rabbit anti-NG2 primary antibody[29] and Alexa Fluor 488 goat antirabbit IgG secondary antibody (Life Technologies), or rat antimouse CD31 primary antibody (BD Biosciences) and Alexa Fluor 488 goat antirat IgG secondary antibody (Life technologies) were used for staining.

Statistical Analyses: All values presented represent mean ± standard deviation. Statistical analysis was performed using the Student's *t*-test or one-way or two-way Analysis Of Variance (ANOVA) followed by posthoc analysis. A value of $P < 0.05$ was considered statistically significant.

Supporting Information

Supporting Information is available from the Wiley Online Library or from the author.

Acknowledgements

This work was supported by grants CA152327 (E.R.), CA188883 (E.R.), CA167174 (K.N.S.) and Cancer Center Support Grant P30 CA030199 from the US National Cancer Institute, and grant 2011CB933600 from the National Basic Research Program of China. The authors thank Venkata R. Kotamraju for peptide synthesis, Junbo Han and Bingkun Chen for the measurements and analysis of two-photon excitation spectra, Sanford Burnham Prebys Histology Core and Flow Cytometry Shared Resource, and IVISR UCSD Moores Cancer Center for the TG imaging. Erkki Ruoslahti is a shareholder of EnduRx Pharmaceuticals, which hold a license to the CGKRK peptide. No potential conflicts of interest were disclosed by the other authors.

Received: August 16, 2015
Revised: October 11, 2015
Published online: December 2, 2015

[1] J. Condeelis, R. Weissleder, *Cold Spring Harbor Perspect. Biol.* **2010**, *2*, a003848.
[2] X. Michalet, F. F. Pinaud, L. A. Bentolila, J. M. Tsay, S. Doose, J. J. Li, G. Sundaresan, A. M. Wu, S. S. Gambhir, S. Weiss, *Science* **2005**, *307*, 538.
[3] a) I. L. Medintz, H. T. Uyeda, E. R. Goldman, H. Mattoussi, *Nat. Mater.* **2005**, *4*, 435; b) Y. Zhu, H. Hong, Z. P. Xu, Z. Li, W. Cai, *Curr. Mol. Med.* **2013**, *13*, 1549.
[4] a) P. Zrazhevskiy, X. H. Gao, *Nat. Commun.* **2013**, *4*, 1619; b) G. S. Hong, J. T. Robinson, Y. J. Zhang, S. Diao, A. L. Antaris, Q. B. Wang, H. J. Dai, *Angew. Chem. Int. Ed.* **2012**, *51*, 9818.
[5] D. R. Larson, W. R. Zipfel, R. M. Williams, S. W. Clark, M. P. Bruchez, F. W. Wise, W. W. Webb, *Science* **2003**, *300*, 1434.
[6] L. Gu, D. J. Hall, Z. T. Qin, E. Anglin, J. Joo, D. J. Mooney, S. B. Howell, M. J. Sailor, *Nat. Commun.* **2013**, *4*, 2326.
[7] H. Z. Zhong, Z. L. Bai, B. S. Zou, *J. Phys. Chem. Lett.* **2012**, *3*, 3167.
[8] H. Mattoussi, G. Palui, H. B. Na, *Adv. Drug Delivery Rev.* **2012**, *64*, 138.
[9] B. A. Rzigalinski, J. S. Strobl, *Toxicol. Appl. Pharmacol.* **2009**, *238*, 280.
[10] L. A. Li, A. Pandey, D. J. Werder, B. P. Khanal, J. M. Pietryga, V. I. Klimov, *J. Am. Chem. Soc.* **2011**, *133*, 1176.
[11] J. Park, C. Dvoracek, K. H. Lee, J. F. Galloway, H. E. C. Bhang, M. G. Pomper, P. C. Searson, *Small* **2011**, *7*, 3148.
[12] A. M. Smith, H. W. Duan, A. M. Mohs, S. M. Nie, *Adv. Drug Delivery Rev.* **2008**, *60*, 1226.
[13] a) D. W. Deng, Y. Q. Chen, J. Cao, J. M. Tian, Z. Y. Qian, S. Achilefu, Y. Q. Gu, *Chem. Mater.* **2012**, *24*, 3029; b) T. Pons, E. Pic, N. Lequeux, E. Cassette, L. Bezdetnaya, F. Guillemin, F. Marchal, B. Dubertret, *ACS Nano* **2010**, *4*, 2531.
[14] E. Ruoslahti, *Adv. Mater.* **2012**, *24*, 3747.
[15] E. Ruoslahti, S. N. Bhatia, M. J. Sailor, *J. Cell Biol.* **2010**, *188*, 759.
[16] J. A. Hoffman, E. Giraudo, M. Singh, L. L. Zhang, M. Inoue, K. Porkka, D. Hanahan, E. Ruoslahti, *Cancer Cell* **2003**, *4*, 383.
[17] L. Agemy, D. Friedmann-Morvinski, V. R. Kotamraju, L. Roth, K. N. Sugahara, O. M. Girard, R. F. Mattrey, I. M. Verma, E. Ruoslahti, *Proc. Natl. Acad. Sci. USA* **2011**, *108*, 17450.
[18] L. Agemy, V. R. Kotamraju, D. Friedmann-Morvinski, S. Sharma, K. N. Sugahara, E. Ruoslahti, *Mol. Ther.* **2013**, *21*, 2195.
[19] H. Dong, N. Dube, J. Y. Shu, J. W. Seo, L. M. Mahakian, K. W. Ferrara, T. Xu, *ACS Nano* **2012**, *6*, 5320.
[20] T. Hayashi, Y. Tanaka, Y. Koide, M. Tanakac, M. Hara, *Phys. Chem. Chem. Phys.* **2012**, *14*, 10196.
[21] T. L. Doane, C. Burda, *Chem. Soc. Rev.* **2012**, *41*, 2885.
[22] E. I. Altinoglu, J. H. Adair, *Wiley Interdiscip. Rev.: Nanomed. Nanobiotechnol.* **2010**, *2*, 461.
[23] A. E. Nel, L. Madler, D. Velegol, T. Xia, E. M. V. Hoek, P. Somasundaran, F. Klaessig, V. Castranova, M. Thompson, *Nat. Mater.* **2009**, *8*, 543.
[24] X. S. Liu, H. Li, Y. J. Chen, Q. Jin, K. F. Ren, J. Ji, *Adv. Healthcare Mater.* **2014**, *3*, 1439.
[25] B. Ballou, B. C. Lagerholm, L. A. Ernst, M. P. Bruchez, A. S. Waggoner, *Bioconjugate Chem.* **2004**, *15*, 79.
[26] H. S. Choi, W. H. Liu, F. B. Liu, K. Nasr, P. Misra, M. G. Bawendi, J. V. Frangioni, *Nat. Nanotechnol.* **2010**, *5*, 42.
[27] H. S. Choi, W. Liu, P. Misra, E. Tanaka, J. P. Zimmer, B. I. Ipe, M. G. Bawendi, J. V. Frangioni, *Nat. Biotechnol.* **2007**, *25*, 1165.
[28] X. Y. Liu, Z. Q. Ye, W. Wei, Y. G. Du, J. L. Yuan, D. Ma, *Chem. Commun.* **2011**, *47*, 8139.
[29] F. J. Huang, W. K. You, P. Bonaldo, T. N. Seyfried, E. B. Pasquale, W. B. Stallcup, *Dev. Biol.* **2010**, *344*, 1035.
[30] H. Z. Zhong, Z. B. Wang, E. Bovero, Z. H. Lu, F. C. J. M. van Veggel, G. D. Scholes, *J. Phys. Chem. C* **2011**, *115*, 12396.
[31] M. N. Wang, X. Y. Liu, C. B. Cao, L. Wang, *J. Mater. Chem.* **2012**, *22*, 21979.
[32] a) X. Y. Liu, W. Wei, C. L. Wang, H. Yue, D. Ma, C. Zhu, G. H. Ma, Y. G. Du, *J. Mater. Chem.* **2011**, *21*, 7105; b) X. Y. Liu, W. Wei, Q. Yuan, X. Zhang, N. Li, Y. G. Du, G. H. Ma, C. H. Yan, D. Ma, *Chem. Commun.* **2012**, *48*, 3155.
[33] Z. G. She, X. Y. Liu, V. R. Kotamraju, E. Ruoslahti, *ACS Nano* **2014**, *8*, 10139.
[34] E. A. Sykes, Q. Dai, K. M. Tsoi, D. M. Hwang, W. C. W. Chan, *Nat. Commun.* **2014**, *5*, 3796.